Impact of potential vorticity intrusions on subtropical upper tropospheric humidity

Darryn W. Waugh

Department of Earth and Planetary Science, Johns Hopkins University, Baltimore, Maryland, USA

Received 6 December 2004; revised 21 February 2005; accepted 1 April 2005; published 4 June 2005.

[1] The impact of Rossby wave breaking on the subtropical tropopause and intrusions of high potential vorticity air into the tropical upper troposphere (UT) on subtropical humidity is examined using measurements from the Microwave Limb Sounder (MLS) and Atmospheric Infrared Sounder (AIRS) satellite instruments and trajectory-based simulations. Both data sets and the simulations show large gradients in humidity in the vicinity of the intrusions, with very dry air within the intrusions (relative humidity (RH) less than 20%) and very moist air ahead (east) of the intrusions (RH around 80%). The dry air within the intrusion is consistent with air from the lowermost stratosphere, while the increase in RH ahead of the intrusions is consistent with the known deep convection and poleward flow in this region, which rapidly transports moist air from the equatorial lower troposphere into the subtropical UT. As the water vapor content of the ambient air in the subtropical UT is already low, the net impact of intrusions is most likely to increase RH in the subtropical UT.

Citation: Waugh, D. W. (2005), Impact of potential vorticity intrusions on subtropical upper tropospheric humidity, *J. Geophys. Res.*, *110*, D11305, doi:10.1029/2004JD005664.

1. Introduction

[2] Earth's climate is particularly sensitive to the water vapor content of the subtropical free troposphere [*Spencer and Braswell*, 1997; *Pierrehumbert*, 2000; *Held and Soden*, 2000], and understanding what controls humidity in this region is important for determining the nature of the water vapor feedback on climate. Observations show that although the subtropical upper troposphere (UT) is dry it is not as dry as expected from the simple picture of subsidence from the top of convective regions, and this implies there must be additional moisture sources for this region [e.g., *Held and Soden*, 2000; *Pierrehumbert*, 2000]. Recent studies indicate that lateral mixing by 'large-scale' advection is the primary source of this additional moisture [e.g., *Salathe and Hartmann*, 1997; *Pierrehumbert*, 1998], and that this mixing is driven by transient wave activity [*Pierrehumbert and Rocca*, 1998]. However, there has only been limited examination of the dynamics behind this transient wave activity and lateral mixing. It is not known what dynamical processes or events are responsible for producing this lateral mixing, or how these processes are modified by changes in the slowly-varying basic state flow. Linking the transport to dynamical processes and answering these questions is important for understanding how the transport, and UT humidity, may be altered by changes in the climate.

[3] A dynamical process that plays a role in lateral mixing in the subtropical UT is Rossby wave breaking on the subtropical tropopause [e.g., *Postel and Hitchman*, 1999; *Waugh and Polvani*, 2000]. In particular, wave breaking during northern winter can produce tongues of stratospheric (high potential vorticity) air that intrude deep into the tropical UT [e.g., *Kiladis and Weickmann*, 1992; *Numaguti*, 1995; *Waugh and Polvani*, 2000; *Waugh and Funatsu*, 2003]. These potential vorticity (PV) intrusions have been linked with transient deep convection in the tropical eastern Pacific [e.g., *Kiladis and Weickmann*, 1992; *Kiladis*, 1998; *Waugh and Funatsu*, 2003], and have been shown to modify subtropical UT ozone [e.g., *Baray et al.*, 2000; *Scott et al.*, 2001; *Waugh and Funatsu*, 2003] and lead to layers of extremely dry air in the lower-middle troposphere in the tropical western Pacific [*Numaguti*, 1995; *Yoneyama and Parsons*, 1999]. However, the impact of these Rossby wave breaking events on upper tropospheric humidity (UTH) has not been quantified.

[4] We examine this issue here using satellite measurements of water vapor together with trajectory-based water vapor simulations. The majority of our analysis focuses on measurements made by the Microwave Limb Sounder (MLS) on the Upper Atmosphere Research Satellite (UARS) [*Read et al.*, 2001], but we also consider more recent measurements by the Atmospheric Infrared Sounder (AIRS) on the Aqua satellite [*Aumann et al.*, 2003]. MLS observations have been used in numerous previous studies to examine a variety of issues regarding UTH, including spatial and temporal variability [*Stone et al.*, 2000], variability related to ENSO [*Newell et al.*, 1997] and the Madden-Julian Oscillation [*Clark et al.*, 1998; *Mote et al.*, 2000], the impact of deep convection [*McCormack et al.*, 2000], and assessment of UTH simulations [*Dessler and Sherwood*, 2000]. However, we are not aware of studies using MLS data to examine any connection between Rossby wave breaking and subtropical UTH.

0148-0227/05/2004JD005664$09.00

[5] The data and model used are described in the next section. In section 3, MLS and AIRS UTH observations and PV from meteorological analyses are used to examine whether there exists any connection between Rossby wave breaking and UTH. The flow and UTH in the vicinity of PV intrusions is then examined in more detail using trajectory simulations in section 4. Concluding remarks are given in the final section.

2. Data and Model

[6] We use version 4.9 MLS measurements [*Read et al.*, 2001] of relative humidity (RH) with respect to ice to examine the UTH distribution. We examine RH rather than absolute humidity as the MLS RH measurements are less affected by temperature errors [*Read et al.*, 2001]. MLS UTH measurements are available on four pressure surfaces between 147 hPa and 464 hPa, but here we consider only measurements on the 215 hPa surface as this surface is close to the 350 K isentropic surface which was the focus of previous studies of PV intrusions [*Waugh and Polvani*, 2000; *Waugh and Funatsu*, 2003]. The accuracy (precision) of MLS 215 hPa RH is 20% (15%) within the tropics [*Read et al.*, 2001]. MLS measurements are made along 15 orbits per day, with measurements every 4.1°. In our analysis we use MLS data binned into a 2.5° latitude by 5° longitude grid as well as individual MLS measurements. The gridded data are used to form maps while the individual measurements are used to examined the detailed UTH structure. MLS UTH measurements commenced in September 1991, with near continuous measurements over the first 3 years and intermittent measurements in later years. We focus here on data from the first 3 northern winters.

[7] Upper tropospheric water vapor has also been measured by the Atmospheric Infrared Sounder (AIRS) instrument on the Aqua satellite [*Aumann et al.*, 2003]. AIRS measures temperature, water vapor and ozone at vertical resolution around 1–2 km and horizontal resolution of 50 km. The AIRS viewing swath is 30 retrieval footprints wide, and the data set includes roughly 300,000 retrieved profiles daily and extends from September 2002 through December 2004. The AIRS water vapor product extends from the surface to about 100 hPa, with minimum sensitivity around 20 ppmv. We focus here on relative humidity (RH) data for the 200 to 250 hPa layer (AIRS constituent data is reported as averages between two levels). RH is not a standard AIRS product but we examine this field for comparison with the above MLS RH measurements. The AIRS RH is constructed from AIRS temperature and water vapor retrievals using the saturation vapor mixing ratio [*Goff and Gratch*, 1946]. In our analysis we use AIRS level 2 (version 3.0) AM and PM orbital data combined into calendar days (0Z to 0Z) and binned into a 1° latitude by 1° longitude grid, which was kindly provided by Andrew Gettelman (NCAR). We examine here AIRS RH measurements from January and February 2003 and 2004. We also briefly examine AIRS ozone for the same layer and period as the water vapor measurements.

[8] Validation of AIRS water vapor and ozone retrievals is not complete. Initial validations have considered only measurements over the oceans and within 40 degrees of the equator, and land data has not been validated [*Fetzer et al.*, 2003]. Furthermore, validation of water vapor retrievals has focused on the middle and lower troposphere (below around 300 hPa), while ozone validation has focused on total column ozone. However, recent comparisons have been made between AIRS and in situ aircraft measurements of upper tropospheric humidity and ozone [*Hagan et al.*, 2004; *Gettelman et al.*, 2004]. These show that AIRS UTH retrievals capture the spatial variability in the aircraft in situ measurements and mixing ratios agree within 25% or better. AIRS ozone also reproduces the spatial variability of the aircraft data, but with a positive bias in the AIRS UT ozone measurements of around 30% [*Gettelman et al.*, 2004]. Preliminary comparisons with in situ ozone measurements from aircraft flights from Hawaii made in January–March 2003 and 2004 [*Ray et al.*, 2004] yield similar conclusions: There is good agreement in spatial structure (in particular the location of the subtropical tropopause and increase in ozone concentrations), but a significant bias for low concentrations (there are in situ measurements as low as 10 ppbv but the AIRS sensitivity threshold appears to be around 70 ppbv).

[9] The occurrence of Rossby wave breaking and the structure of the resulting intrusions is examined using potential vorticity (PV) calculated from National Center for Environmental (NCEP)/National Center for Atmospheric Research (NCAR) reanalysis data [*Kalnay et al.*, 1996]. These data have 2.5° latitude by 2.5° longitude resolution and are available 6-hourly. We also use the winds from these reanalyses to examine the horizontal and vertical motion, and to calculate trajectories in the water vapor simulations.

[10] The water vapor simulations performed use the trajectory-based model of *Dessler and Sherwood* [2000] (similar calculations have been performed by *Salathe and Hartmann* [1997], *Pierrehumbert* [1998], and *Pierrehumbert and Rocca* [1998]). In this model a water vapor tracer is carried along three-dimensional trajectories, and is conserved except when the relative humidity (RH) reaches 100%, at which point the water content is reduced in order to maintain the relative humidity at 100% and all the condensed water falls out immediately. This means that the water vapor concentration at the end of a trajectory is given by the minimum saturation mixing ratio encountered along the trajectory. The sensitivity of the simulated RH to the assumption of instant removal of water when RH equals 100% has been examined by *Dessler and Sherwood* [2000], and using a different critical value or a delay in the precipitation cause only relatively small differences in RH and will not alter any of the conclusions drawn in this study.

[11] In the calculations presented below, 6-hourly archived horizontal and vertical winds from the NCEP/NCAR reanalyses are used to calculate the parcel trajectories, and the saturation mixing ratios along the trajectories are determined using reanalysis temperatures. Twenty-day back trajectories are performed, and the water vapor is given by minimum saturation mixing ratio over those twenty days. In the few cases when the minimum occurs at the end of the back trajectory (i.e. 20 days before target day) we assume, as in *Dessler and Sherwood* [2000], the water vapor content equal to an initial RH of 50%. The results presented are insensitive to this assumption. The back trajectories used in the model are initialized at the location of MLS UTH measurements for that day. However, the trajectories

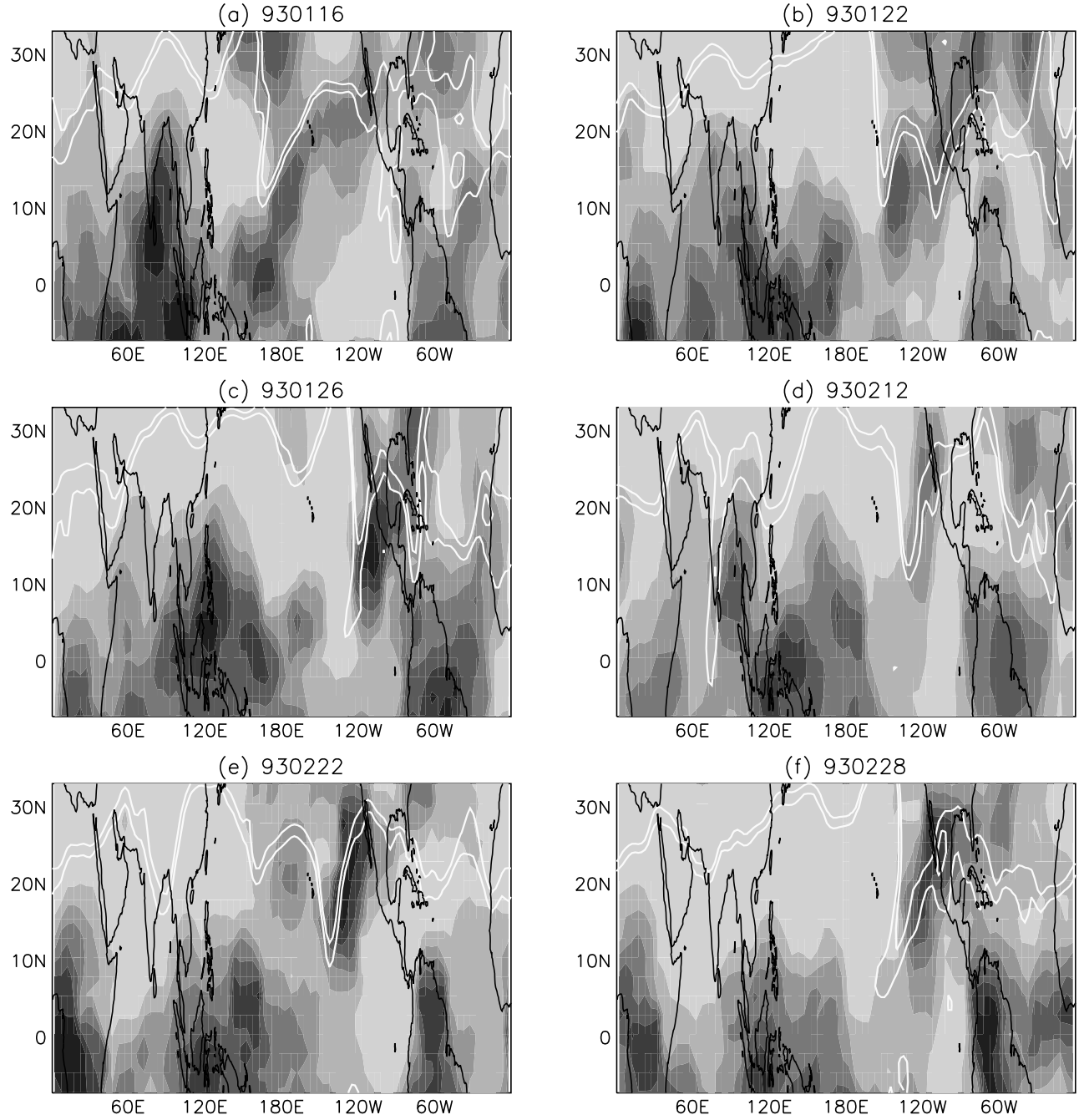

Figure 1. Maps of MLS 215 hPa RH (shading) and NCEP 350K PV (contours) for several days in January and February 1993. The shading interval for the RH is 20% with lightest shading corresponding to RH < 20% and darkest shading to RH > 120%. Contours show PV = 1 and 2 PVU.

are started at 12Z and not at the actual MLS measurement time.

3. Water Vapor Observations

[12] We first examine daily maps of MLS 215 hPa RH, and investigate whether there is any signal of PV intrusions. We focus on northern subtropics during winter, as PV intrusions are well defined in the northern hemisphere and occur most often in winter [*Waugh and Polvani*, 2000].

[13] Figure 1 shows maps of MLS 215 hPa RH for several days in January and February 1993. These maps show that there are large variations in the subtropics. In particular, in the northern subtropical Pacific (120E–120W) there is a background of very low RH (less than 20%) which is interrupted by tongues of much higher RH (above 80%) reaching from the equator into the subtropics. The moist tongues are most likely of much finer scale than can be resolved by the 2.5° by 5° gridded MLS data shown in Figure 1. For example, trajectory-based simulations of *Pierrehumbert* [1998] show a background of dry air which is interrupted by very fine-scale moist plumes.

[14] Also shown in Figure 1 are the PV = 1 and 2 PVU contours (1 PVU = 10^{-6} m^2 s^{-1} kg^{-1} K) on the 350 K

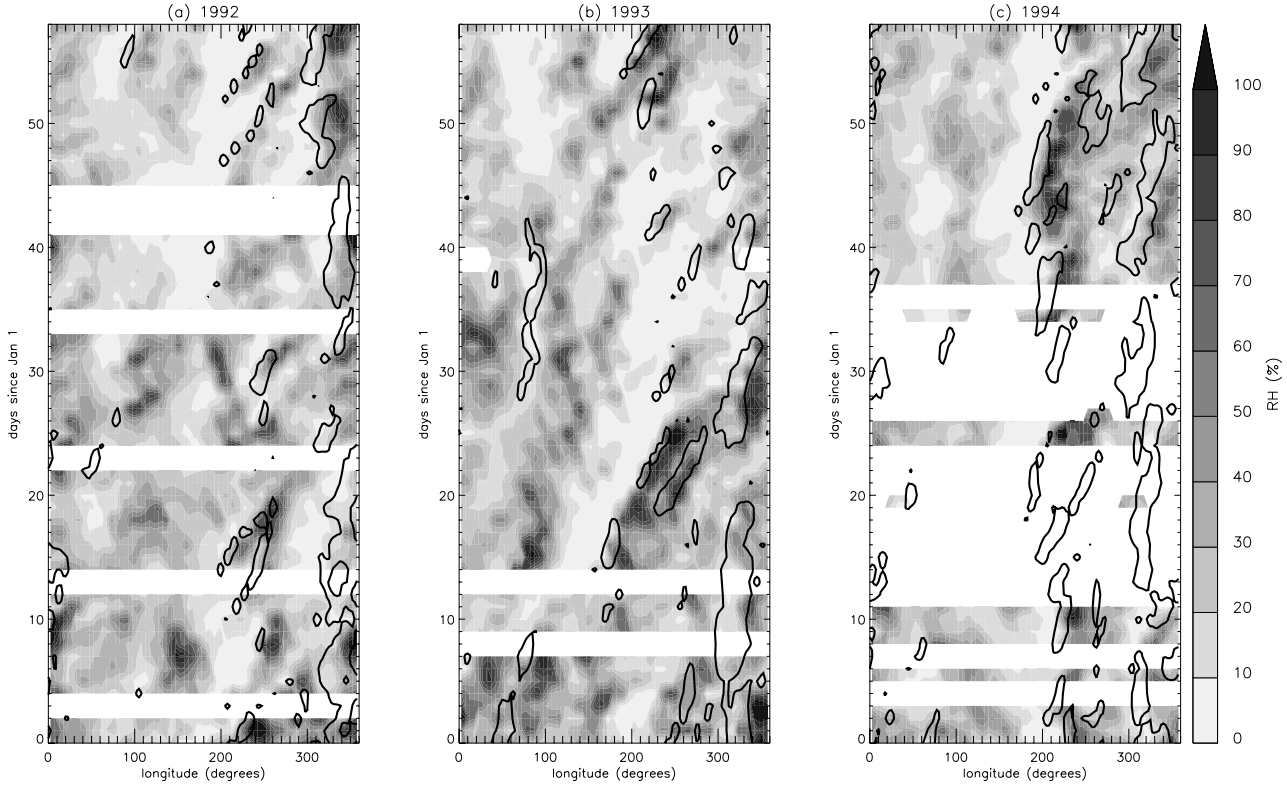

Figure 2. Longitude-time variation of MLS 215 hPa RH at 16.25°N for January–February in 1992, 1993, and 1994. Contours show PV = 1.5 PVU at 17.5°N. White horizontal lines in Figure 2b mark dates shown in Figure 1. See color version of this figure at back of this issue.

isentropic surface. These show that for the days shown there are intrusions of high-PV air into the tropical Pacific. Examination of sequences of 6-hourly PV data shows that these intrusions are transient features and are the result of subtropical Rossby wave breaking [*Waugh and Polvani*, 2000; *Waugh and Funatsu*, 2003]. As is typical for Rossby wave breaking on the subtropical tropopause during northern winter, the PV fields show, in each case, that a disturbance propagated eastward along the the region of steep meridional PV gradients (the tropopause), amplified as in it entered the region of weaker winds over the Pacific, and produced a narrow tongue of high PV with almost north-south orientation. See *Waugh and Polvani* [2000] and *Waugh and Funatsu* [2003] for more detailed discussion of the dynamics of these wave breaking events. (Note that it is not always clear from the analysed PV that there is irreversible deformation of PV contours, and hence Rossby wave breaking. However, high resolution transport calculations show significant filamentation and deformation of contours not observed in the analyses [e.g., *Scott et al.*, 2001] and indicate that there is indeed Rossby wave breaking during these events.)

[15] Comparison of the PV contours in Figure 1 with the RH suggests that some of the variability in RH may be related to the occurrence of PV intrusions. In particular, there is generally a region of moist air ahead (east) of a PV intrusion with much drier air behind (west of) the PV intrusion, e.g., around 180°E on 16 January and around 120°W on 26 January.

[16] To examine this connection further, we show in Figure 2 the longitude-time variation of 215 hPa RH at 16.25°N (shading) and 350 K PV at 17.5°N (contours) for January–February 1992 to 1994. The sporadic occurrence of PV greater than 1.5 PVU marks the occurrence of PV intrusions. For example, the intrusions shown in Figure 1 appear as PV contours around 180E (January 16), 220E (January 22) or 240E (January 26, February 12, 22, 28) in Figure 2b (the horizontal white lines show these dates). PV intrusions can be seen at all longitudes in Figure 2, but generally occur over the eastern Pacific (200–240E) and Atlantic (300–360E) Oceans. This is consistent with the climatology of *Waugh and Polvani* [2000] (although most of the intrusions shown in Figure 2 do not meet the criteria of PV $\geq$2 PVU at 10N used in *Waugh and Polvani* [2000]). In nearly every instance of high PV shown in Figure 2 there is high RH to the east of the PV, confirming the link between intrusions and high subtropical RH. Figure 2 also shows that there is very low RH to the west of the high PV.

[17] This link between PV intrusions and increases in subtropical RH is also seen in AIRS data. For example, Figure 3a shows the same quantities as in Figure 2, except using AIRS data for 2004. (In this plot we have filled in missing data by interpolating in longitude.) The same features as in Figure 2 can be seen in Figure 3a: There is a sporadic occurrence of high PV, with high values of RH occurring immediately to the east of these events and low values to the west. A clear signal of low RH within the PV intrusions can also be seen in Figure 3a. This is expected as the air within the intrusions comes from the stratosphere. Low values inside the intrusion are not, however, seen in the MLS plots (Figures 1 and 2). This is because of the low horizontal resolution of the MLS data (i.e. few measure-

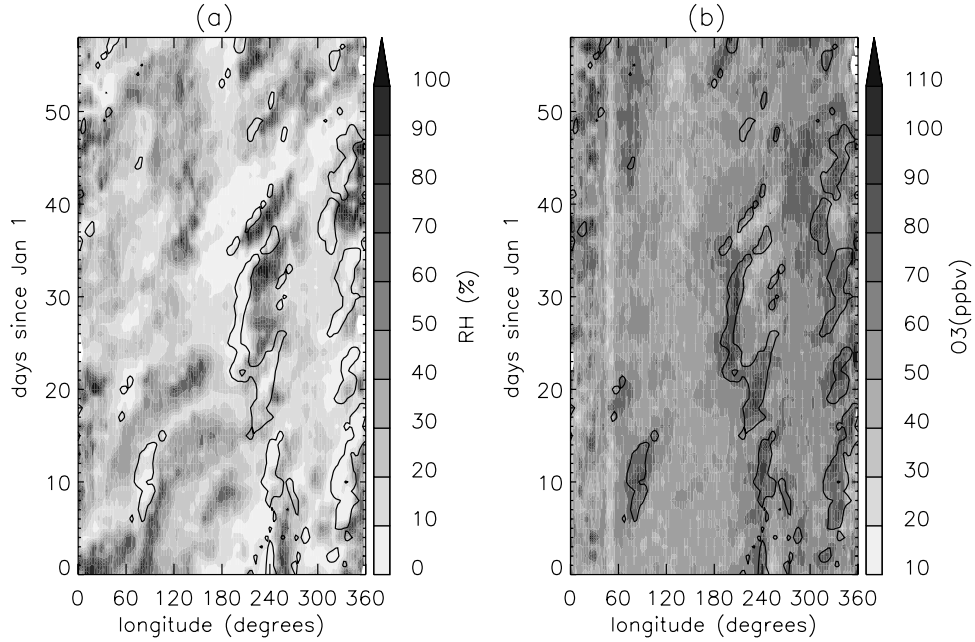

Figure 3. Longitude-time variation of AIRS 200–250 hPa (a) RH and (b) O_3 mixing ratios at 17.5°N for January–February in 2004. Contours show PV = 1.5 PVU at 17.5°N. See color version of this figure at back of this issue.

ments within the intrusions) and the 2.5° latitude by 5° longitude averaging used to make the gridded data (see further discussion below).

[18] To examine the variation of RH in the vicinity of intrusions in more detail we form composite-mean RH fields for PV intrusion events over the northern Pacific. Intrusion events during the MLS and AIRS periods are identified in a similar manner to *Waugh and Polvani* [2000]: All occurrences where PV $\geq$ 2.5 PVU at 17.5°N (as opposed to PV $\geq$ 2 PVU at 10°N in Waugh and Polvani) were identified, and all occurrences within 10° longitude or within 6 days were grouped together as a single intrusion event. Using this criteria there were 20 intrusion events during the MLS period (January–February 1992 to 1994) and 18 events during the AIRS period (January–February 2003 and 2004). The mean MLS or AIRS RH field is then calculated for the central day of these events. To account for shifts in the location of the intrusions when forming the composites, the fields were shifted in longitude so that all intrusions occurred at the same longitude (210°E). Figure 4 shows the longitudinal variations of the composite-mean MLS (dashed curve) and AIRS (solid curve) RH.

[19] Figure 4 confirms that there is low RH to the west (behind) and high RH (ahead) to the east of PV intrusions. Furthermore, it shows there is excellent agreement between the MLS and AIRS measurements, with both data sets showing RH around 70–80% ahead of the intrusions and RH around 10–20% behind the intrusions. There is a difference in the increase in RH at the central longitude. This is due to the limited spatial resolution of MLS and averaging/interpolation used to form the gridded data. (Examination of individual MLS profiles shows few measurements close to centre of intrusions.) We repeated the composite analysis using individual MLS profiles, rather than the gridded data, and averaged the data into 10° bins. The resulting composite-mean RH (symbols in Figure 4) shows a much larger west-east gradient at the central longitude, and better agreement with the AIRS composite. Also, both the composite-means based on AIRS data and individual MLS profiles show a minimum in RH just west of the central longitude. Although the difference between

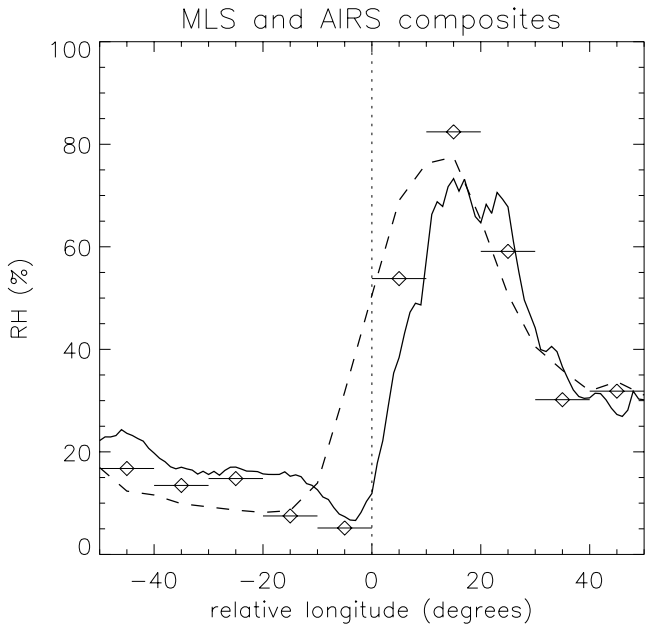

Figure 4. Longitudinal variation of the composite-mean RH for north Pacific intrusion events in January–February, for AIRS (solid curve) and MLS (dashed curve) measurements in 2003–2004 and 1992–1994, respectively. Diamonds and horizontal lines show MLS composite using individual profile data rather than gridded data. Longitude is relative to longitude of the PV intrusion (vertical dotted line).

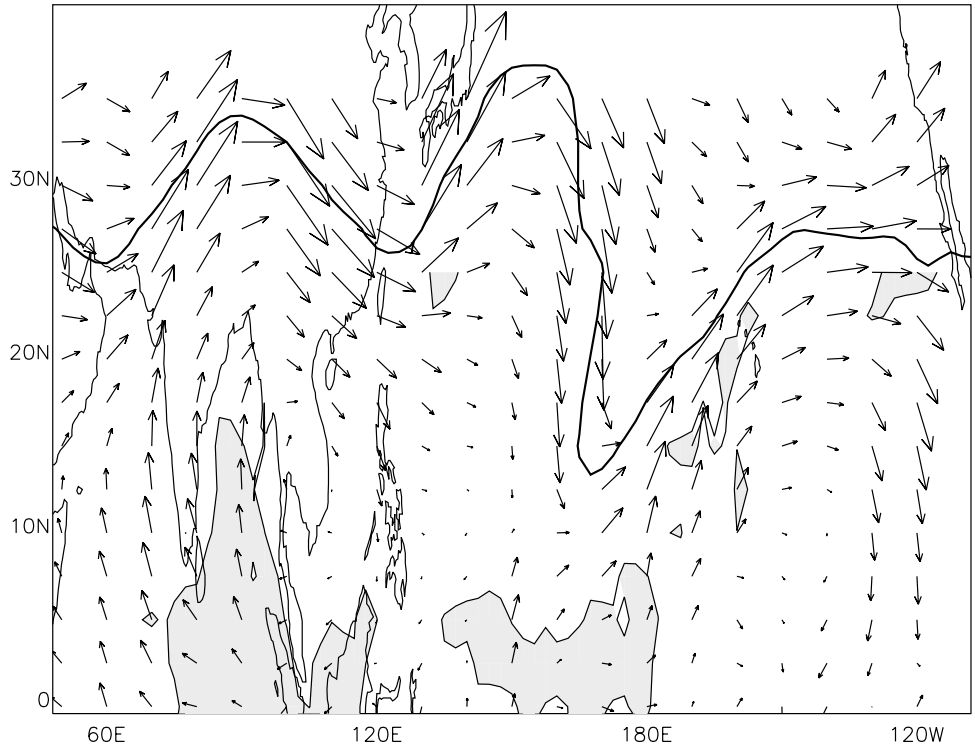

Figure 5. Map of isentropic flow on 350 K surface for 16 January 1993. Thick contour is PV = 2 PVU and thin contour and shading is OLR less than 200 W/m^2. The OLR data are the NOAA spatially and temporally interpolated OLR [*Liebmann and Smith*, 1996].

the minimum and the RH further to the west is small, and these low humidity values are near (or below) the sensitivity of the MLS and AIRS instruments.

[20] The above figures show a close link between PV intrusions and increases in subtropical RH, but say nothing about causality. However, consideration of the expected flow due to a PV intrusion suggests that the intrusion causes the increase in RH. Theoretically it is expected that there will be reduced stability, ascent, and poleward flow ahead of upper level PV anomalies [e.g., *Hoskins et al.*, 1985], and this is found in the meteorological analyses (e.g., Figure 5). This reduced stability and ascent initiates (and supports) convection ahead of the PV anomaly. Deep convection (e.g., low outgoing longwave radiation (OLR)) is indeed observed ahead of the PV intrusions [*Kiladis*, 1998; *Waugh and Funatsu*, 2003], e.g., Figure 5, and more detailed analysis and model calculations confirms that the intrusions cause the convection (B. Funatsu, personal communication, 2005). The combination of convection and poleward flow ahead of the PV intrusion rapidly transports lower tropospheric air into the subtropical UT (see trajectories in next section). This then produces the observed tongues of high RH. Note that the low OLR and high RH are both observed around 10 to 15 degrees to the east of the PV tongue; see *Waugh and Funatsu* [2003, Figure 7b] and Figure 2.

[21] The above analysis indicates that transport associated with intrusion events have a large impact on subtropical UTH. We would also expect this transport to alter the concentrations of ozone, and other trace constituents, in the subtropical UT. In particular, we would expect high concentration of ozone (typical of the lowermost stratosphere) within the intrusions but low concentrations (typical of the clean boundary layer) ahead of the intrusions. Such differences were noted by *Waugh and Funatsu* [2003] in their analysis of ozonesondes from Hilo, Hawaii (e.g., see their Figure 12). This increase of ozone within intrusions also occurs in the AIRS data, see Figure 3b. In all cases, the AIRS 200–250 hPa ozone exceeds 80 ppbv (and often 110 ppbv) within the regions of high PV. There is also a hint of low ozone ahead of some of the intrusions, e.g., intrusions around 200–240°E in early January and early February. A composite analysis of AIRS ozone, similar to that of RH shown in Figure 4, yields a composite-mean peak around 100 ppbv within the intrusion and a minimum around 55 ppbv around 15° east (ahead) of the intrusion. However, as discussed in section 2, there are large biases in AIRS ozone for low concentrations, and the minimum ozone ahead of the intrusion is likely lower than in the AIRS data. (The persistent low values of ozone around 50°E in Figure 3b should be disregarded as these correspond to retrievals over Saudi Arabia and AIRS retrievals have not been validated over land and the retrievals are known to be more problematic over warm, desert surfaces.)

[22] Although Figures 2 and 3a show a clear connection between PV intrusions and high RH they also show there are occurrences of high subtropical RH that are unrelated to the PV intrusions, e.g., over the western and central Pacific (90° to 180°E). The high AIRS RH are also generally accompanied by low ozone concentrations. In the western subtropical Pacific there is poleward flow as part of the subtropical anticyclonic flow (Figure 5), and this transports air from equatorial convective regions into the subtropics in a manner similar to the flow ahead of the intrusions, also producing moist tongues extending from the equator into

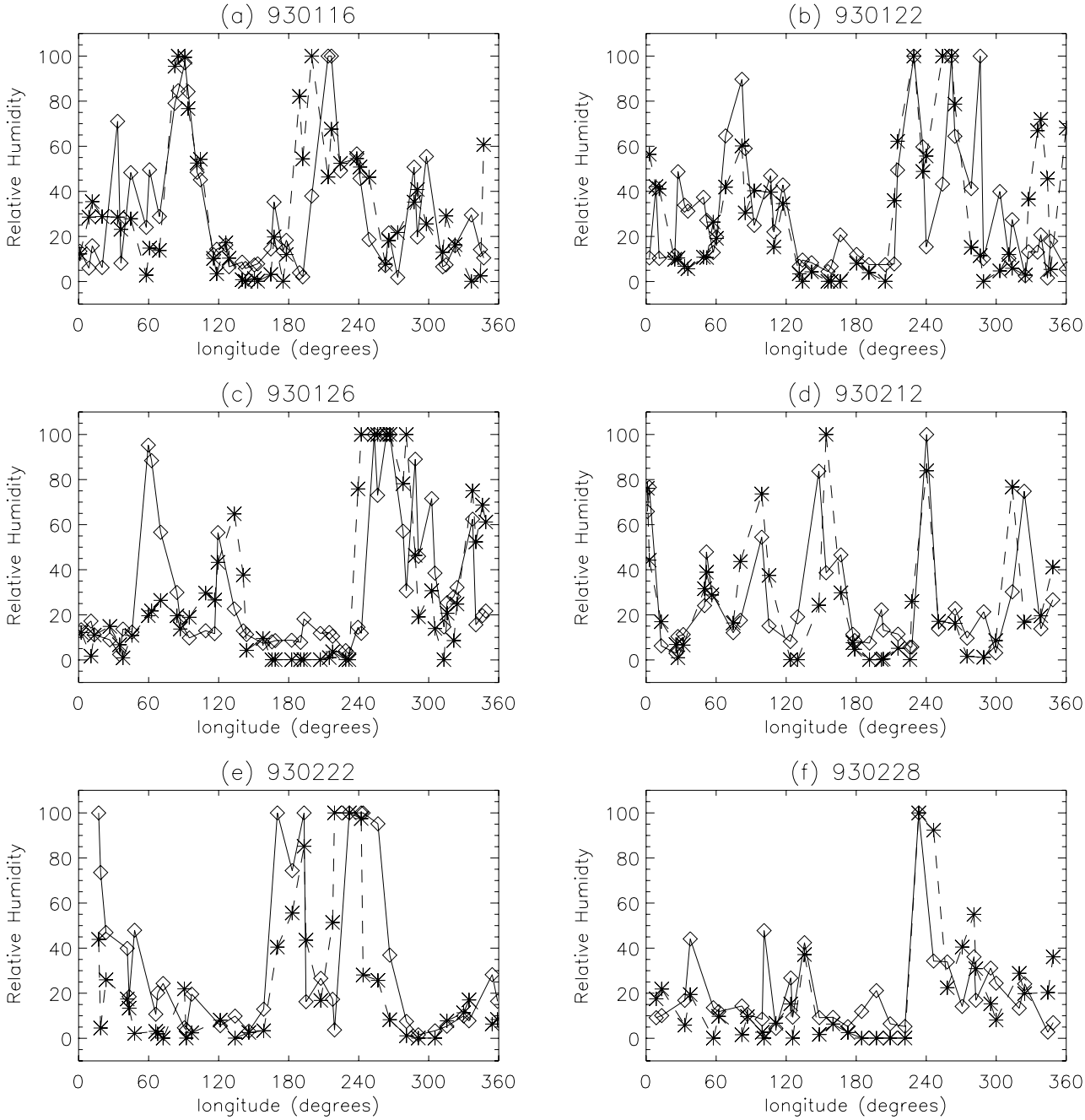

Figure 6. Comparison of model (diamonds and solid lines) and MLS (asterisk and dashed lines) 215 hPa RH for latitudes between 17° and 21°N, for days shown in Figure 1.

the subtropics (e.g., Figure 1a). The causes of the temporal variations in these moist tongues deserves investigation, but is beyond the scope of this study.

4. Water Vapor Simulations

[23] We now use trajectory-based UTH simulations to examine in more detail the cause of the regions of low and high UTH in the vicinity of PV intrusions. As described in section 2, the model used is the same as that of *Dessler and Sherwood* [2000]. They showed that there was good agreement between modeled and MLS UTH for monthly-averaged fields, at 4° latitude by 5° longitude resolution. Here we compare the model with daily MLS observations with no spatial averaging. For each day considered the model back-trajectories are initialized, and hence RH determined, at the location of the MLS measurements. The back trajectories were however initialized at 12Z, and not at the actual time of the MLS measurements. We focus on the RH distributions for the dates shown in Figure 1.

[24] Figure 6 compares the longitudinal variation of RH between 17° and 21° N from the model and MLS observations, for the days shown in Figure 1. (In these plots, MLS measurements of RH above 100% are replaced by 100%.) These plots again show large meridional gradients in the observed RH, with variations over 80% occurring between

neighboring measurements. The simulations also show large variability, and although there are differences in detail (e.g., at low values the model is generally higher than the observations) the overall agreement between model and data is reasonable. The cross-correlation coefficients calculated for each day are around 0.5 to 0.6. These correlations are significant at greater than 99% confidence level (i.e., there is greater than 99% confidence that the computed correlations did not arise from the comparison of two random uncorrelated samples). More importantly, for this analysis, the simulated tongues of moist air are generally of similar width and location as observed.

[25] There are many possible reasons for the differences shown in Figure 6. These include measurement errors (around 20% [*Read et al.*, 2001]), the limited vertical resolutions (3–4 km) and large horizontal footprint of MLS measurements, the temporal offset between model and measurements, missing microphysical processes in the model, errors in the meteorological fields (trajectories), and unresolved motions (i.e., no small-scale convective motion). The errors are likely amplified by the fine-scale structure in UT humidity, and the fact that small differences in location or spatial averaging can produce large differences. While a detailed model-data comparison and sensitivity analysis is warranted we leave this for a future study, possibly involving measurements from AIRS and Aura MLS [*Waters et al.*, 1999]. The general agreement shown in Figure 6 is sufficient to give us confidence that we can use these model simulations to examine differences in the source/pathways of the air masses in the vicinity of PV intrusions.

[26] As in the observations, the model shows high RH ahead of the PV intrusion but low RH behind the intrusion. These differences can be understood in terms of the different pathways and temperature histories of the different air masses. To examine these different histories we examine ensembles of trajectories with similar characteristics. This analysis is similar to the analysis of ''coherent ensemble of trajectories'' in extratropical cyclones by *Wernli and Davies* [1997] and *Wernli* [1997]. Here we group the trajectories depending on their location relative to the PV tongue and their simulated RH. In particular, we consider three types of parcels: (1) parcels whose back trajectory starts behind the intrusion and whose RH is less than 20%, (2) parcels within the intrusion with RH less than 20%, and (3) parcels ahead of the intrusion with RH greater than 60%.

[27] Figure 7 shows the history of the location and temperature of each of these groups of air parcels, for the 6 intrusions shown in Figure 1. The trajectories within each category (behind, within, or ahead of the intrusion) are very similar, especially the horizontal motion. There are, however, clear and important differences between the trajectories of each category. As expected from PV and velocity fields the air ahead, within, and behind the intrusion have come from very different locations (Figures 7a–7c). (In the horizontal maps the longitude of each event was shifted so that the PV intrusion occurred at the same notional longitude (210°E).) The air ahead and behind of the intrusion comes from lower latitudes, but whereas the air ahead of the intrusion has come directly from equatorial regions the air behind is swept out of western equatorial Pacific (100–150°E), by the subtropical anticyclone, into the subtropics and then east and south to the final location. The originating location of air within the intrusion has, in contrast to air ahead or behind, remained in the subtropics for the preceding 5 days and sampled a larger longitude range. For earlier times (5 to 10 days before) there is more variation in the trajectories of these parcels, with some trajectories remaining in extratropics while others come from the tropics (and even the southern hemisphere).

[28] More importantly, for understanding the water vapor content, are differences in the vertical motion of the air (Figures 7d–7f). The air within and behind the PV intrusions has (in general) slowly descended over the preceding 5–10 days, whereas the air ahead of the intrusions has ascended rapidly from the lower troposphere over the preceding 3–5 days. (The modeled vertical motion ahead of the intrusion is likely underestimated, because of lack of small-scale convective motion in the model.) The rapid ascent for air ahead of the intrusion is consistent with the observations of convection ahead of intrusions (e.g., Figure 5). Although the air behind and within the intrusion has all descended from pressures around or below 150 hPa there is variability in the time when the air reached these low pressures: Air behind the intrusion reaches these pressures 5 to 10 days before, whereas that inside the intrusion reached the same pressures 10 to 20 days before (not shown).

[29] The above differences in vertical motion result in different temperature histories (Figures 7g–7i) and minimum saturation mixing ratios (not shown), and hence different water vapor content. The air ahead of the intrusion rapidly cools as it ascends and becomes (and often remains) saturated, and this produces the high modeled, and observed, RH ahead of the intrusion. In contrast the air behind and within the intrusion warms as it descends and the water vapor mixing ratio is set by the cold temperatures (around 205 K) encounter 5 or more days previously. As the water vapor content remains constant as the air warms the RH decreases to very low values, and is independent of the time since last saturated.

[30] The parcel histories shown in Figure 7 explain not only the observed difference in RH ahead and within the intrusion but also the similar values within and behind the intrusion. Although air within and behind the PV intrusion can have very different horizontal path histories they have similar minimum pressures and temperatures over the preceding 20 days, and as a result their water vapor content are very similar. There can be differences in time and location of last saturation (the saturation of air behind the intrusion occurs within 10 degrees of the equator whereas the saturation of air within the intrusions occurs anywhere from 10°S to 35°N), but in all cases the air has passed through a cold region (temperature less than 210 K) and has very low water vapor content.

5. Concluding Remarks

[31] Analysis of upper tropospheric humidity (UTH) from measurements by the MLS and AIRS satellite instruments and trajectory-based simulations has shown that there is high relative humidity (RH > 80%) ahead (east) of potential vorticity (PV) intrusions into the northern subtropics. This is consistent with the known deep convection and poleward flow ahead of these intrusions [*Kiladis*, 1998; *Waugh and*

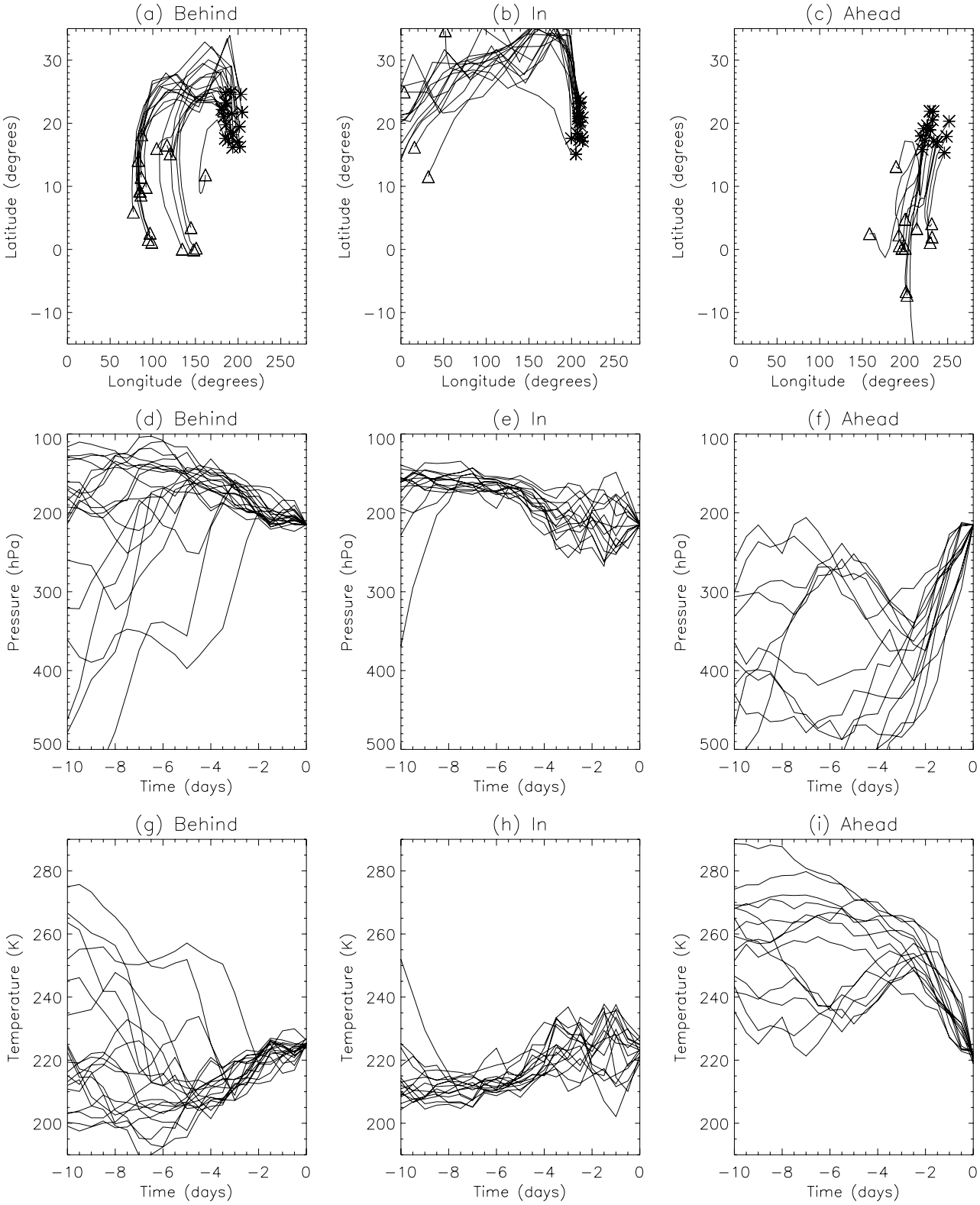

Figure 7. Temporal evolution of (a–c) horizontal location, (d–f) pressure, and (g–i) temperature of air parcels behind (left panels), within (middle), and ahead (right) of PV intrusions. In Figures 7a–7c the final location is shown as an asterisk, the location five days earlier as a triangle, and the longitude of events have been shifted so that in all events the intrusion occurs at 210°E.

Funatsu, 2003], which rapidly transports moist air from the equatorial lower troposphere into the subtropical UT. Dry, stratospheric air (RH < 20%) is also transported into the subtropical UT within the intrusions, although the amount of irreversible transport in unknown. As a result there are strong gradient in UTH associated with the intrusions. There are also strong gradients in UT ozone, with high ozone within the intrusions and low ozone (from the marine boundary layer) ahead of the intrusion.

[32] As the dynamics of intrusions, and in particular the dependence on the basic state flow, is reasonably well known the above connection between intrusions and water vapor transport provides some insight into spatial and temporal variations in subtropical UTH. As the water vapor content of lowermost stratospheric air is similar to ambient subtropical UT air the transport within the intrusions will have only a small impact on subtropical UTH, and the net impact of intrusions on subtropical UTH is likely to be an increase due to transport ahead of the intrusions. Intrusions occur more frequently in regions where the subtropical jet is weak and there are equatorial westerlies [*Waugh and Polvani*, 2000], and from the above arguments we expect increased subtropical UTH in these regions. The spatial distribution of climatological northern winter RH is consistent with this expectation as the maxima in the northern subtropical RH occurs at the downstream edges of the regions with frequent intrusions (around 240°E and 360°E) [*Read et al.*, 2001; *Bates et al.*, 2001]. The observed interannual and intraseasonal variations in the northern subtropical eastern Pacific are also consistent with the above expectations. In this region there is an increase in UTH in the phases of the El Nino Southern Oscillation (ENSO) and Madden Julian Oscillation (MJO) when the subtropical jet is weaker and equatorial westerlies stronger over the Pacific, i.e., during La Nina years [*Bates et al.*, 2001; *McCarthy and Toumi*, 2004] and during the phase of MJO with enhanced convection over the east Indian Ocean [*Sassi et al.*, 2002]. Note, although the variability in RH is consistent with changes in intrusion frequency we cannot say the RH changes are definitely due to changes in intrusions as other processes that influence the RH also vary with ENSO and the MJO. For example, some of this ENSO-variability in RH may, as argued by *McCarthy and Toumi* [2004], be due to changes in temperature that are independent of transport.

[33] The strong gradients in UT water vapor and ozone in the vicinity of the subtropical intrusions resemble the gradients observed in association with midlatitude tropopause folds; see, e.g., *Olson and Stanford* [2001] and *Wimmers and Moody* [2004a, 2004b] where these gradients are used to identify midlatitude folds. However, there are significant differences in the dynamics and transport of subtropical intrusions and midlatitude folds. In the midlatitude case there is strong baroclinicity, with deep downward penetration of the high-PV tongue and mutual interaction of this with a surface front [e.g., *Hoskins et al.*, 1985], whereas the subtropical intrusions are fairly barotropic, do not penetrate into the lower troposphere [*Waugh and Funatsu*, 2003], and have little interaction with surface fronts (B. Funatsu, personal communication, 2005). (Note, some strong midlatitude events reach into the subtropics but maintain the typical characteristics of midlatitude intrusions, e.g., deep downward penetrate troposphere and interaction with surface lows (e.g., O. R. Cooper et al., Direct transport of midlatitude stratospheric ozone into the lower troposphere and marine boundary layer of the tropical Pacific Ocean, submitted to *Journal of Geophysical Research*, 2005).) As a result, whereas the dry, high-ozone air in a midlatitude fold descends into the middle/lower troposphere the corresponding air in subtropical intrusions generally remains in the UT. There are also differences in the ascent of moist, boundary layer air ahead of the PV tongues. In midlatitude systems this ascending air is typically part of a warm conveyor belt [*Browning*, 1990], where advection plays an important role in the ascent up a frontal surface and the upward transport can occur over large distances (e.g., 30 degrees latitude) [e.g., *Wernli*, 1997; *Cooper et al.*, 2002; *Esler et al.*, 2003]. In contrast the ascent ahead of subtropical intrusions occurs in deep convection, and within a localized region.

[34] The analysis here has focused on water vapor around 215 hPa during northern winter intrusions. It would be interesting to examine the impact of Rossby wave breaking and intrusions during other seasons, and at other altitudes. At lower altitudes the air within intrusions may be much drier than the ambient subtropical air, and the net impact of the intrusions on subtropical moisture could differ. It would also be interesting to examine other dynamical processes that transport moisture into the subtropical UT. For example, as shown here (Figures 1–3), there are occurrences of high subtropical UTH that appear to be produced by the poleward component of the subtropical anticyclones rather than by intrusions. The examination of the above issues will be enhanced by further analysis of AIRS measurements as well as measurements from the new MLS instrument on the Aura satellite [*Waters et al.*, 1999].

[35] **Acknowledgments.** We thank Bill Read for the gridded MLS data, Andrew Gettelman for the AIRS data, Paul Newman for access to NCEP/NCAR and MLS data, and Andy Dessler for the trajectory-based water vapor model. We also thank Andy Dessler, Andrew Gettelman, Ann Marie Eldering, Eric Fetzer, and Bill Irion for helpful comments and discussions. The NOAA spatially and temporally interpolated OLR were obtained from the NOAA-CIRES Climate Diagnostics Center (http://www.cdc.noaa.gov/). This work was supported by NSF grant ATM-0094971 and NASA grant NAG5-11283.

References

Aumann, H. H., et al. (2003), AIRS/AMSU/HSB on the Aqua Mission: Design, science objectives and data products, *IEEE Trans. Geosci. Remote Sens.*, *41*, 253–264.

Baray, J. L., V. Daniel, G. Ancellet, and B. Legras (2000), Planetary-scale tropopause folds in the southern subtropics, *Geophys. Res. Lett.*, *27*, 353–356.

Bates, J. J., D. L. Jackson, F.-M. Breon, and Z. D. Bergen (2001), Variability of tropical upper tropospheric humidity 1979–1998, *J. Geophys. Res.*, *106*, 32,271–32,281.

Browning, K. E. (1990), Organisation of clouds and precipitation in extratropical cyclones, in *Extratropical Cyclones - The Erik Palmen Memorial Volume*, pp. 129–153, Am. Meteorol. Soc., Boston, Mass.

Clark, H. L., R. S. Harwood, P. W. Mote, and W. G. Read (1998), Variability of water vapor in the tropical upper troposphere as measured by the Microwave Limb Sounder on UARS, *J. Geophys. Res.*, *103*, 31,695–31,707.

Cooper, O. R., et al. (2002), Trace gas composition of midlatitude cyclones over the western North Atlantic Ocean: A conceptual model, *J. Geophys. Res.*, *107*(D7), 4056, doi:10.1029/2001JD000901.

Dessler, A., and S. C. Sherwood (2000), Simulations of tropical upper tropospheric humidity, *J. Geophys. Res.*, *105*, 20,155–20,163.

Esler, J. G., et al. (2003), Transport and mixing between air masses in cold frontal regions during Dynamics and Chemistry of Frontal Zones (DCFZ), *J. Geophys. Res.*, *108*(D4), 4142, doi:10.1029/2001JD001494.

Fetzer, E. et al. (2003), Validation of AIRS/AMSU/HSB core products for Data Release Version 3.0, *JPL Publ.*, *D-26538*.

Gettelman, A., et al. (2004), Validation of Aqua satellite data in the upper troposphere and lower stratosphere with in situ aircraft instruments, *Geophys. Res. Lett.*, *31*, L22107, doi:10.1029/2004GL020730.

Goff, J. A., and S. Gratch (1946), Low-pressure properties of water from −160F to 212F, *Trans. Am. Soc. Heat. Vent. Eng.*, *52*, 95–121.

Hagan, D. E., et al. (2004), Validating AIRS upper atmosphere water vapor retrievals using aircraft and balloon in situ measurements, *Geophys. Res. Lett.*, *31*, L21103, doi:10.1029/2004GL020302.

Held, I. M., and B. J. Soden (2000), Water vapor feedback and global warming, *Ann. Rev. Energy Environ.*, *25*, 441–475.

Hoskins, B. J., M. E. McIntyre, and A. W. Robertson (1985), On the use and significance of isentropic potential vorticity maps, *Q. J. R. Meteorol. Soc.*, *111*, 877–946. (Also *Q. J. R. Meteorol. Soc.*, *113*, 402–404, 1985.)

Kalnay, E., et al. (1996), The NCEP/NCAR 40-year reanalysis project, *Bull. Am. Meteorol. Soc.*, *77*, 437–471.

Kiladis, G. N. (1998), Observations of Rossby waves linked to convection over the eastern tropical Pacific, *J. Atmos. Sci.*, *55*, 321–339.

Kiladis, G. N., and K. M. Weickmann (1992), Extratropical forcing of tropical Pacific convection during northern winter, *Mon. Weather Rev.*, *120*, 1924–1938.

Liebmann, B., and C. A. Smith (1996), Description of a complete (interpolated) outgoing longwave radiation data set, *Bull. Am. Meteorol. Soc.*, *77*, 1275–1277.

McCarthy, M. P., and R. Toumi (2004), Observed interannual variability of tropical troposphere relative humidity, *J. Clim.*, *17*, 3181–3191.

McCormack, J., R. Fu, and W. B. Read (2000), The impact of tropical deep convection on the upper tropospheric water vapor based on UARS MLS measurements, *Geophys. Res. Lett.*, *27*, 525–528.

Mote, P. W., H. L. Clark, T. J. Dunkerton, R. S. Harwood, and H. C. Pumphrey (2000), Intraseasonal variations of water vapor in the tropical upper troposphere and tropopause region, *J. Geophys. Res.*, *105*, 17,457–17,470.

Newell, R. E., Y. Zhu, W. G. Read, and J. W. Waters (1997), Relationship between tropical upper tropospheric moisture and eastern tropical Pacific sea surface temperature at seasonal and interannual time scales, *Geophys. Res. Lett.*, *24*, 25–28.

Numaguti, A. (1995), Characteristics of 4-to-30-day period disturbances in the tropical Pacific region, *J. Meteorol. Soc. Jpn.*, *48*, 47–59.

Olson, M. A., and J. L. Stanford (2001), Evidence of stratospheric-to-troposphere transport within a mesoscale model and Total Ozone Mapping Spectrometer total ozone, *J. Geophys. Res.*, *106*, 27,323–27,334.

Pierrehumbert, R. T. (1998), Lateral mixing as a source of subtropical water vapor, *Geophys. Res. Lett.*, *25*, 1784–1806.

Pierrehumbert, R. T. (2000), Subtropical water vapor as a mediator of rapid global climate change, in *Mechanisms of Global Change at Millennial Timescales*, *Geophys. Monogr. Ser.*, edited by P. U. Clark, R. S. Webb, and L. D. Keigwin, AGU, Washington, D. C.

Pierrehumbert, R. T., and R. Rocca (1998), Evidence for control of Atlantic subtropical humidity by large scale advection, *Geophys. Res. Lett.*, *25*, 4537–4540.

Postel, G. A., and M. H. Hitchman (1999), A climatology of Rossby wave breaking along the subtropical tropopause, *J. Atmos. Sci.*, *56*, 359–373.

Ray, E. A., K. H. Rosenlof, E. Richard, D. Parrish, and R. Jakoubek (2004), Distributions of ozone in the region of the subtropica jet: An analysis of in situ aircraft measurements, *J. Geophys. Res.*, *109*, D08106, doi:10.1029/2003JD004143.

Read, W. G., et al. (2001), UARS Microwave Limb Sounder upper tropospheric humidity measurement: Method and validation, *J. Geophys. Res.*, *106*, 32,207–32,258.

Salathe, E. P., and D. L. Hartmann (1997), A trajectory analysis of tropical upper-tropospheric moisture and convection, *J. Clim.*, *10*, 2533–2547.

Sassi, F., M. Salby, H. C. Pumphrey, and W. G. Read (2002), Influence of the Madden-Julain Oscillation on upper tropospheric humidity, *J. Geophys. Res.*, *107*(D23), 4681, doi:10.1029/2001JD001331.

Scott, R. K., J. P. Cammas, P. Mascart, and C. Stolle (2001), Stratospheric filamentation into the upper tropical troposphere, *J. Geophys. Res.*, *106*, 11,835–11,848.

Spencer, R. W., and W. D. Braswell (1997), How dry is the tropical free troposphere? implication for global warming theory, *Bull. Am. Meteorol. Soc.*, *78*, 1097–1106.

Stone, E. M., L. Pan, B. J. Sandor, W. G. Read, and J. W. Waters (2000), Spatial distributions of upper tropospheric water vapor measurements from UARS Microwave Limb Sounder, *J. Geophys. Res.*, *105*, 12,149–12,161.

Waters, J., et al. (1999), The UARS and EOS Microwave Limb Sounder experiments, *J. Atmos. Sci.*, *56*, 194–218.

Waugh, D. W., and B. M. Funatsu (2003), Intrusions into tropical upper troposphere: Three dimensional structure and accompanying ozone and OLR distributions, *J. Atmos. Sci.*, *60*, 637–653.

Waugh, D. W., and L. M. Polvani (2000), Intrusions into the tropical upper troposphere, *Geophys. Res. Lett.*, *27*, 3857–3860.

Wernli, H. (1997), A Lagrangian-based analysis of extratropical cyclones. 2. A detailed case-study, *Q. J. R. Meteorol. Soc.*, *123*, 1677–1706.

Wernli, H., and H. C. Davies (1997), A Lagrangian-based analysis of extratropical cyclones. 1. The method and some applications, *Q. J. R. Meteorol. Soc.*, *123*, 467–489.

Wimmers, A. J., and J. L. Moody (2004a), Tropopause folding at satellite-observed spatial gradients: 1. Verification of an empirical relationship, *J. Geophys. Res.*, *109*, D19306, doi:10.1029/2003JD004145.

Wimmers, A. J., and J. L. Moody (2004b), Tropopause folding at satellite-observed spatial gradients: 2. Development of an empirical model, *J. Geophys. Res.*, *109*, D19307, doi:10.1029/2003JD004146.

Yoneyama, K., and D. B. Parsons (1999), A proposed mechanism for the intrusion of dry air into the tropical western pacific region, *J. Atmos. Sci.*, *56*, 1524–1546.

D. W. Waugh, Department of Earth and Planetary Science, Johns Hopkins University, Baltimore, MD 21218, USA. (waugh@jhu.edu)

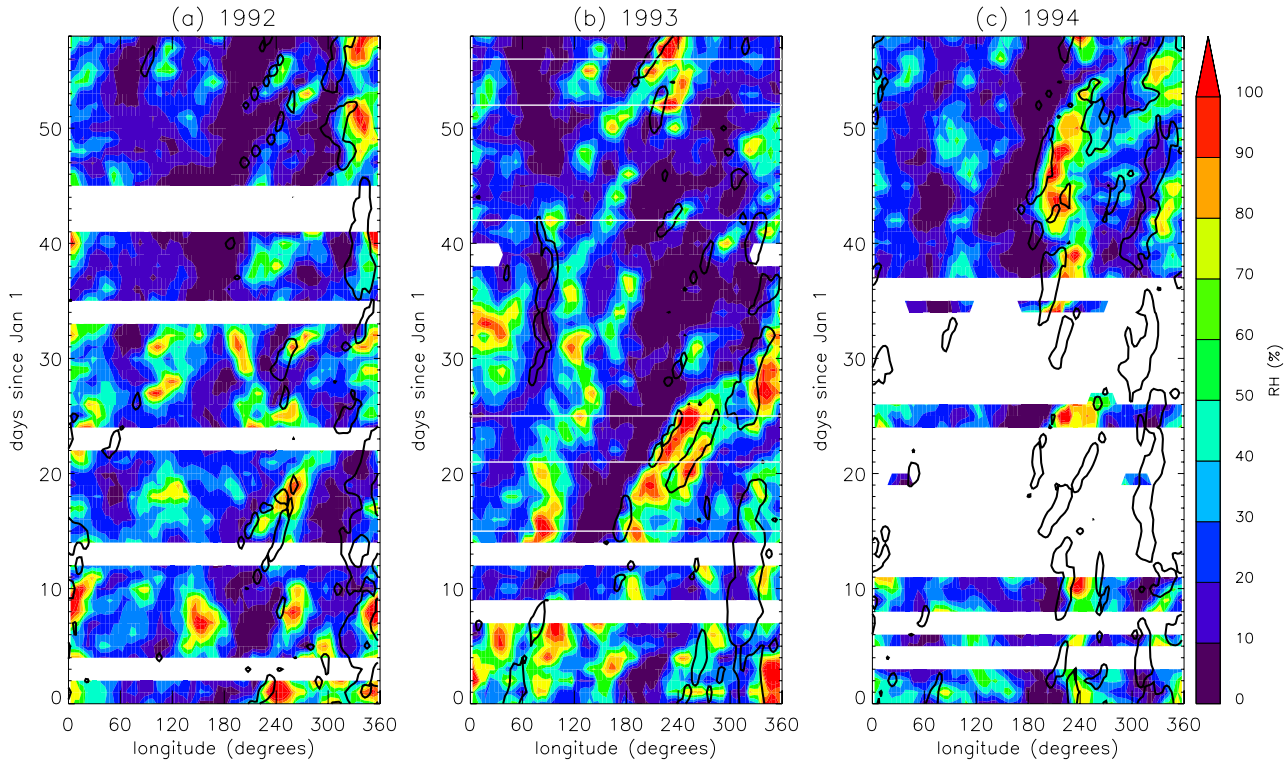

Figure 2. Longitude-time variation of MLS 215 hPa RH at 16.25°N for January–February in 1992, 1993, and 1994. Contours show PV = 1.5 PVU at 17.5°N. White horizontal lines in Figure 2b mark dates shown in Figure 1.

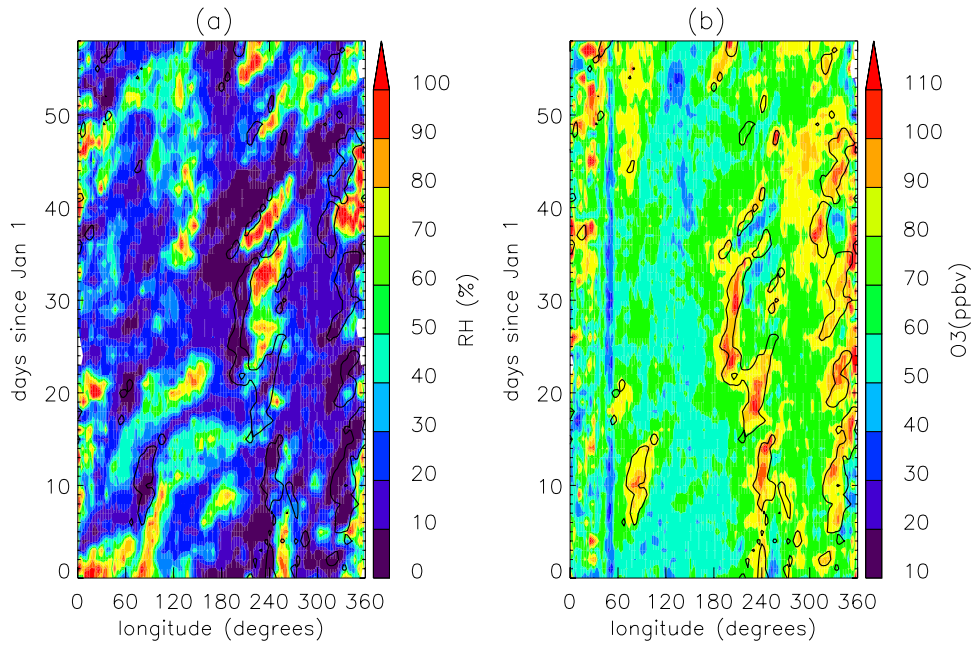

Figure 3. Longitude-time variation of AIRS 200–250 hPa (a) RH and (b) O_3 mixing ratios at 17.5°N for January–February in 2004. Contours show PV = 1.5 PVU at 17.5°N.